

1 Clear-water scour depth prediction in long channel contractions: 2 Application of new hybrid machine learning algorithms

3 Khabat Khosravi*¹, Mir Jafar Sadegh Safari², James R.Cooper³

4 1. Department of Watershed Management Engineering, Ferdowsi University of Mashhad, Mashhad, Iran.

5 2. Department of Civil Engineering, Yaşar University, Izmir, Turkey. Email: jafar.safari@yasar.edu.tr

6 3. School of Environmental Sciences, University of Liverpool, Liverpool, UK. Email:
7 james.cooper@liverpool.ac.uk

8
9

10 *Corresponding author: K. Khosravi (Khabat.khosravi@gmail.com and kh.khosravi@um.ac.ir)

11 Abstract

12 Scour depth prediction and its prevention is one of the most important issues in channel and
13 waterway design. However the potential for machine learning algorithms to provide models
14 of scour depth has yet to be explored. This study provides the first quantification of the
15 predictive power of a range of standalone and hybrid machine learning models. Using
16 previously collected scour depth data from laboratory flume experiments, the performance of
17 five types of recently developed standalone machine learning techniques - the Isotonic
18 Regression (ISOR), Sequential Minimal Optimization (SMO), Iterative Classifier Optimizer
19 (ICO), Locally Weighted learning (LWL) and Least Median of Squares Regression (LMS) -
20 are assessed, along with their hybrid versions with Dagging (DA) and Random Subspace
21 (RS) algorithms. The main findings are five-fold. First, the DA-ICO model had the highest
22 prediction power. Second, the hybrid models had a higher prediction power than standalone
23 models. Third, all algorithms underestimated the maximum scour depth, except DA-ICO
24 which predicted scour depth almost perfectly. Fourth, scour depth was most sensitive to
25 densimetric particle Froude number followed by the non-dimensionalized contraction width,
26 flow depth within the contraction, sediment geometric standard deviation, approach flow
27 velocity and median grain size. Fifth, most of the algorithms performed best when all the
28 input parameters were involved in the building of the model. An important exception was the
29 best performing model that required only four input parameters: densimetric particle Froude

30 number, non-dimensionalized contraction width, flow depth within the contraction and
31 sediment geometric standard deviation. Overall the results revealed that hybrid machine
32 learning algorithms provide more accurate predictions of scour depth than empirical
33 equations and traditional AI-algorithms. In particular, the DA-ICO model not only created the
34 most accurate predictions but also used the fewest easily and readily measured input
35 parameters. Thus this type of model could be of real benefit to practicing engineers required
36 to estimate maximum scour depth when designing in-channel structures.

37

38 **Keywords:** Scour depth prediction; data mining; iterative classifier optimizer algorithms;
39 model calibration

40

41 **1. Introduction**

42 Channel contractions in rivers exist when there is a reduction in the width of the cross-
43 section. The length of the contraction is defined based on the ratio between the length of the
44 contracted area (L) and the width of the channel upstream of the contracted area (b_1 , approach
45 width), although the criterion for defining whether a contraction is ‘long’ varies between
46 researchers. For example Komura (1966) defined contractions as being long if the ratio was
47 above unity, Webby (1984) if it was greater than two, and Raikar (2004) stated the
48 contraction could only be considered long if the flow velocity and turbulence remained
49 constant in the length of the contraction when $L/b_1 \geq 1$. Natural contractions in alluvial rivers,
50 such as debris accumulations, longitudinal bars and confluences, tend to be long contractions,
51 since the flow is nearly uniform in both the undisturbed channel and the contracted reach.
52 Human made examples include gradual contractions created on both sides of the channel to
53 accommodate dams, bridges, weirs and barrages, and partial constrictions on one side of the
54 channel such as spur dikes or cofferdams (Lim, 1993).

55 Local scour at the contraction occurs because of a local increase in flow velocity and bed
56 shear stress. The severity of this scour varies according to upstream sediment supply
57 conditions, and thus the scour is categorized into two main groups, clear-water and live-bed
58 scour (Dey and Raikar, 2005). Clear-water scour takes place when sediment transport occurs
59 from the scour hole throughout the contraction length and when there is no upstream
60 sediment supply. Live-bed scour takes place when there is upstream sediment supply (Dey,
61 1997).

62 To successfully design in-channel structures, the maximum scour depth, which is mainly
63 caused by constriction (Lim, 1993), must be predicted because the depth dictates
64 morphological change around the structure, especially in long contractions, and thus the
65 structure's stability. This prediction is commonly made under the assumption of an
66 equilibrium condition (Lim and Cheng, 1998). The first analytical study of scour depth
67 prediction in this condition in a long contraction was carried out by Straub (1934), and
68 subsequent studies have either proposed different empirical equations or modified Straub's
69 equation (Laursen, 1960; Ashida, 1963; Komura, 1966; Gill, 1981; Webby, 1984; Lim, 1993;
70 Lim and Cheng, 1998). For example, Lim (1993) revealed that previously incorporated
71 effective variables in clear-water scour depth equations were inadequate and therefore
72 proposed a new empirical formula for long contraction based on the approach flow velocity
73 and depth, median grain size of the bed material and the geometry of the constriction. In a
74 following study, Lim and Cheng (1998) revealed Straub's equation underestimates scour
75 depth in both clear-water and live-bed conditions, and proposed a new empirical formula
76 based on only the approach water depth and the ratio between the approach and constricted
77 channel width. Dey and Raikar (2005) used an experimental approach to investigate the
78 controlling variables on scour depth for uniform and graded sediments. They found that
79 Lim's (1993) equation over predicted scour depth and developed their own empirical

80 equation based on the limiting stability of bed sediments in the approaching channel under
81 clear-water scour. These examples illustrate that a range of equations exist, all based on
82 differing controlling variables, and each performing differently according to the channel and
83 flow conditions being studied. No universal equation exists to predict scour depth well in all
84 conditions. One possible reason is the proposed scour depth relationships were developed
85 using conventional regression analysis.

86 Recently artificial intelligence (AI) algorithms have gained much interest because of their
87 non-linear structure (Maier et al. 2014), superior prediction power - particularly for complex
88 phenomena - shorter computational times, low sensitivity to missing values, and their ability
89 to handle large datasets with different temporal and spatial scales (Melesse et al, 2011;
90 Yaseen et al. 2016). These AI based algorithms have been widely used in the fields of water
91 science and hydraulic engineering. Artificial neural network (ANN) algorithms are one of the
92 most widely used (Abrahart et al. 2012). ANN was found initially to successfully predict
93 scour depth around hydraulic structures (Muzzammil, 2008; Mousa, 2013; Onen, 2014), but
94 recent studies have shown low prediction capability if the training datasets are not carefully
95 selected (Melesse et al, 2011; Kisi et al, 2012; Choubin et al, 2018), especially when the
96 range of testing data is out of range of the training dataset (low generalization power).

97 To predict scour depth around hydraulic structures, Adaptive neuro-fuzzy inference system
98 (ANFIS) algorithms have been developed by integrating ANN with fuzzy logic (Firat, 2009;
99 Rady, 2020). One of the key challenges in developing an accurate ANFIS models is
100 determining accurately the weights in the membership function of the ANFIS algorithm
101 (Chen et al. 2017; Bui et al. 2016)..

102 Alternative types of AI-based algorithms have been successfully applied and proposed for
103 scour depth prediction. For example, Guven and Gunal (2008) and Azamathulla et al. (2010)

104 reported that genetic programming (GP) outperforms conventional regression and ANN
105 approaches. Ayoubloo et al. (2010) showed the classification and regression trees (CART)
106 algorithm is more accurate for scour modeling than the ANN method. Furthermore, Etemad-
107 Shahidi and Ghaemi (2011) examined the potential of two other AI-based algorithms,
108 Support vector machine (SVM) and M5 model tree. Their work found the M5 model tree
109 algorithm outperformed ANN and SVM approaches. Ghaleh Nou et al. (2019) also found the
110 same results for self-adaptive extreme learning machine in comparison to SVM and ANN
111 approaches. One possible reason is SVM algorithms have many hyperparameters that require
112 tuning and thus finding the best combination is a challenge. Whereas Parsaie et al. (2019)
113 showed that SVM provided more accurate predictions than ANN and ANFIS approaches.
114 However, Najafzadeh et al. (2016) reported the superiority of the ANFIS to SVM, revealing
115 further that the performance of AI-based algorithms are sensitive to the dataset, and thus
116 fluvial conditions, used to build them. Najafzadeh et al. (2013, 2014) explored the influence
117 of hybridization by applying Neuro-fuzzy group method of data handling (GMDH) systems
118 based evolutionary algorithms to predict scour pile groups in clear water conditions. Their
119 work revealed the integration of these models with evolutionary algorithms enhanced model
120 performance. In a subsequent study, Najafzadeh et al. (2018) applied three algorithms of gene
121 expression programming (GEP), model tree (MT) and evolutionary polynomial regression
122 (EPR) to reveal that the MT algorithm had a higher prediction power than GEP and EPR in
123 long channel contractions. This work was developed further by revealing the performance of
124 a hybrid model - GMDH hybridized with GEP - was greater than the standalone ANN, GEP
125 and GMDH algorithms (Najafzadeh and Saberi-Movahed, 2019). In these studies, almost all
126 of the AI-based algorithms provided more accurate predictions of scour depth than empirical
127 equations.

128 Recently a new branch of AI algorithms, called machine learning, have been developed,
129 providing strong performance in other environmental and engineering fields. For example, in
130 the field of landslide prediction, stochastic gradient descent (SGD), AdaBoost (AB), logistic
131 model tree (LMT), functional tree (FT), Naïve Bayes Tree (NBT), Bayes network (BN), and
132 Naïve Bayes (NB) algorithms have been successfully applied (Bui et al. 2019a; Pham et al.
133 2019). LMT, REPT and Alternating Decision Trees (ADT) algorithms have provided strong
134 prediction of flood maps (Khosravi et al. 2018a; Chapi et al. 2017), and ADT and AB
135 algorithms have proved successful in the prediction of groundwater potential (Bui et al.
136 2019b). Further, Khosravi et al. (2018b) and Salih et al. (2019) have applied BA-M5P,
137 attribute selected classifier (AS), M5Rule (M5R), KStar, instance-based learning (IBK),
138 random committee-REPT (RC-REPT) and random subspace-REPT (RS-REPT) to predict
139 suspended sediment loads. Decision trees algorithms have been used to predict reference
140 evaporation (Khosravi et al., 2019), apparent shear stress in compound channels (Khozani et
141 al., 2019) and solar radiation (Sharafati et al., 2019). Khosravi et al. (2020a) predicted
142 fluoride concentration in groundwater through IBK and locally weighted learning (LWL)
143 algorithms. Khosravi et al. (2020b) developed hybrid algorithms of bagging (BA) with
144 decision trees algorithm (BA-M5P), random forest (BA-RF), random tree (BA-RT) and
145 reduced error pruning tree (BA-REPT) for bed load transport rate prediction. Nitrate and
146 strontium concentration has been predicted using Gaussian Process (GP) algorithms (Bui et
147 al, 2020a), and water quality indices have been simulated using a hybrid of BA, CV
148 parameter selection (CVPS) and randomizable filtered classification (RFC) with decision
149 trees algorithms (Bui et al. 2020b). All of these previous studies have shown that hybrid
150 algorithms have a higher prediction power then their standalone counterparts, but they have
151 yet to be applied to the prediction of scour depth.

152 Thus the aim of this study was to evaluate the ability of hybrid machine learning algorithms
153 to provide accurate predictions of maximum scour depth. The focus was on scour within long
154 contractions within clear-water conditions. Five standalone machine learning algorithms -
155 Isotonic Regression (ISOR), Sequential Minimal Optimization (SMO), Iterative Classifier
156 Optimizer (ICO), Locally Weighted learning (LWL) and Least Median of Squares Regression
157 (LMS) - were hybridized with Dagging (DA) and Random Subspace (RS) algorithms to
158 develop 10 novel hybrid algorithms DA-ISOR, DA-SMOR, DA-LWL, DA-ICO, DA-LMS, -
159 ISOR, RS-SMOR, RS-LWL, RS-ICO, RS-LMS). This study is the first to apply a diverse
160 range of newly developed machine learning models to the prediction of scour depth. The
161 research offers new insight into which machine learning algorithms offer the potential to
162 provide accurate and efficient predictions of scour depth based on readily and easily
163 measured flow and channel variables.

164 **2. Methodology**

165 **2.1. Identifying effective parameters**

166 According to the literature, the parameters which have a significant effect on scour depth in a
167 long contraction can be classified into four different types (Straub, 1934; Laursen, 1960;
168 Ashida, 1963; Komura, 1966; Gill, 1981; Webby, 1984; Lim, 1993; Lim and Cheng, 1998;
169 Raikar, 2004): (1) approaching flow conditions (flow velocity U_1 , critical flow velocity U_c ,
170 flow depth h_1 , water density ρ_w , densimetric particle Froude number Fr_0); (2) characteristics
171 of the bed material characteristics (median grain size d_{50} , sediment density ρ_s , sediment
172 geometric standard deviation σ_g); (3) geometry of the un-contracted section (width b_1 , h_1);
173 and (4) geometry of the contracted (width b_2 , flow depth h_2) section. The functional
174 relationship of scour depth (d_s) with these effective input parameters can be described as
175 follows:

$$176 \quad d_s = f(U_1, U_c, \rho_w, d_{50}, \rho_s, \sigma_g, b_1, h_1, b_2, g) \quad (1)$$

177 To enhance the modeling performance of the AI-based algorithms (Azamathulla et al. 2009;
 178 Pal et al. 2014) and allow direct comparisons between datasets and the results of previous
 179 studies, all parameters were non-dimensionalized. Such an approach is recommended in the
 180 application of AI algorithms because it improves model performance (Azamathulla et al.
 181 2009; Pal et al. 2014). Since there are a large number of variables, a non-dimensional
 182 approach was also required in the use of the Buckingham π theorem to determine groupings
 183 between parameters. Also more generally, finding a functional relationship among non-
 184 dimensional parameters can allow a practical model to be developed to mitigate the adverse
 185 consequences of the experimental data scale effects.

186

187 Applying the Buckingham π theorem and using $\Delta\rho = \rho_s - \rho_w$ instead of ρ_s , and taking U_1, b_1
 188 and ρ as repeating variables, allows the following dimensionless parameters to be obtained.

$$189 \quad f(d_s/b_1, U_1/U_c, d_{50}/b_1, b_2/b_1, h_1/b_1, \Delta\rho/\rho, U_1^2/gb_1, \sigma_g) = 0 \quad (2)$$

190 Combining the three π parameters of $U_1^2/gb_1, d_{50}/b_1$ and $\Delta\rho/\rho$ as $[(U_1^2/gb_1) \times$
 191 $(d_{50}/b_1)^{-1}/(\Delta\rho/\rho)]^{0.5}$ gives

$$192 \quad Fr_0 = \frac{U_1}{\sqrt{g((\rho_s/\rho_w)^{-1})d_{50}}} \quad (3)$$

193 where Fr_0 is the densimetric particle Froude number. Using the Buckingham theorem, six
 194 dimensionless parameters were extracted as having the most effect on scour depth. Thus the
 195 scour depth was normalized using b_1 and the effective variables were extracted as follows:

$$196 \quad d_s/b_1 = f(U_1/U_c, Fr_0, d_{50}/b_1, b_2/b_1, h_1/b_1, \sigma_g) \quad (4)$$

197 Eq. (4) shows all effective variables given in Eq. (1) are appropriately incorporated as
 198 dimensionless model parameters. In order to compute scour depth as a dependent variable,

219 d_s/b_1 is considered as a model output and dimensionless parameters given in the right hand
 200 side of Eq. (4) are used as model inputs. The form of Eq. (4) is in agreement with that used
 201 for scour depth determination by Dey and Raikar (2005) and Najafzadeh et al. (2018).

202

203 2.2. Dataset collection and preparation

204 In the current study 204 datasets from four laboratory flume studies, collected and compiled
 205 by Najafzadeh et al. (2016, 2018) for the testing of standalone learning algorithms, were used
 206 (Kamura, 1966; Gill, 1981; Webby, 1984; Lim, 1993; and Dey and Raikar, 2005). All of the
 207 data were measured in a long contraction rectangular channel in a clear-water condition. The
 208 datasets were divided into three sections randomly. Among the 204 datasets, 70% (140 row-
 209 data) was used as a training dataset for model building, 10% for calibration (22 row-data) and
 210 the remaining 20% (42 row-data) for model validation. A statistical summary of the datasets
 211 is presented in Table 1.

212

Table 1. Descriptive statistics of utilized data

Parameters	Training					Calibration					Testing				
	Max	Min	Mean	STD	Skew	Max	Min	Mean	STD	Skew	Max	Min	Mean	STD	Skew
h_1/b_1															
b_2/b_1	0.23	0.04	0.14	0.05	-0.21	0.22	0.07	0.14	0.06	-0.21	0.23	0.06	0.15	0.06	-0.22
Fr_0	0.70	0.25	0.53	0.13	-0.36	0.70	0.25	0.53	0.13	-0.51	0.70	0.25	0.54	0.13	-0.51
U_p/U_c	5.05	0.11	0.60	0.57	4.77	2.34	0.12	0.57	0.34	1.17	1.52	0.12	0.55	0.34	1.07
σ_g	1.00	0.39	0.89	0.12	-2.40	1.00	0.55	0.90	0.10	-2.44	1.00	0.55	0.90	0.10	-2.44
d_s/b_1	23.75	0.88	7.54	7.06	1.01	23.75	0.88	7.52	7.01	1.01	23.75	0.88	7.52	7.01	1.01

213

214 2.3. Best input combination and sensitivity analysis

215 Apart from dataset quality, the correct selection of the input parameters has the largest impact
 216 on model performance. As explained in the application of the Buckingham π theorem, six

217 different dimensionless parameters were obtained from the effective variables involved. In
 218 order to understand the influence of individual dimensionless parameters on model
 219 performance, different input combinations were evaluated. This influence was determined by
 220 examining the correlation coefficient (r) between the input parameters and output (d_s/b_1)
 221 (Table 2) for different input combinations (Table 3). The input combinations were
 222 constructed by first using the input parameter with the highest correlation coefficient (Fr_0 ;
 223 combination No. 1), and then creating subsequent combinations by adding each time the
 224 parameter with the next highest r until the parameter with the lowest r was finally added
 225 (combination No. 6). This approach is the common way of determining the most effective
 226 input parameters (Yaseen et al, 2016; Khozani et al, 2019; Salih et al, 2019). At first, each
 227 developed algorithm was tested using all the input combinations and with default model
 228 parameter values to determine the best input combination. Once complete, a sensitivity
 229 analysis, examining the effect of each parameter on scour depth, was performed) using the
 230 testing dataset.

231 Table 2. Correlation coefficients between input variables and scour depth

Input Variables	h_1/b_1	b_2/b_1	Fr_0	U_V/U_c	d_{50}/b_1	σ_g
r	0.563	-0.578	-0.624	0.330	0.292	0.331

232

233 Table 3. Different input combinations used to model scour depth

No.	Different input combination	Output
1	Fr_0	d_s/b_1
2	$Fr_0, b_2/b_1$	d_s/b_1
3	$Fr_0, b_2/b_1, h_1/b_1$	d_s/b_1
4	$Fr_0, b_2/b_1, h_1/b_1, \sigma_g$	d_s/b_1
5	$Fr_0, b_2/b_1, h_1/b_1, \sigma_g, U_V/U_c$	d_s/b_1
6	$Fr_0, b_2/b_1, h_1/b_1, \sigma_g, U_V/U_c, d_{50}/b_1$	d_s/b_1

234

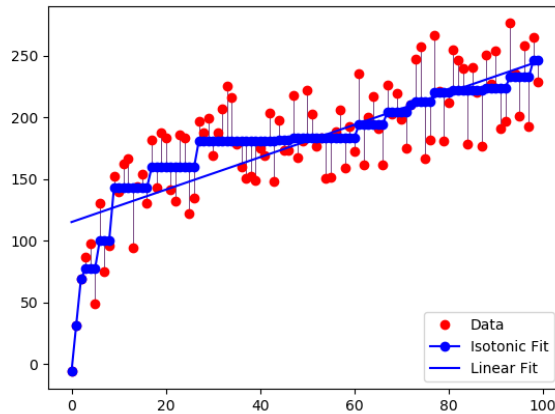
235 **2.4. Models parameter optimization**

236 The determination of the optimum values for each model parameter has a great effect on the
237 models predictive power. Optimal parameter values differ from study to study and there is
238 not a global optimum value; hence, in any study, identifying optimal model parameters is an
239 important step in the model building process. In the current study optimal values were
240 determined using the widely accepted trial-and-error approach, and the calibration dataset
241 (Choubin et al, 2018; Sherafati et al, 2019). The root mean square error (*RMSE*) metric was
242 used for determination of the optimum value, as the lower the *RMSE* for the testing phase, the
243 more effective the model performance. Optimum values for each machine learning algorithm,
244 along with some key definitions, are presented in Table A and B in the supplementary
245 materials.

246 **2.5. Model theory background**

247 **2.5.1. Isotonic Regression (ISOR)**

248 Isotonic Regression (ISOR), which is also called monotonic regression, is an approach, like
249 any form of regression, of fitting a line through the measured data but a number of rules and
250 restrictions apply. For example, the fitting line (isotonic curve) must be non-decreasing/non-
251 increasing and has to be the closest distance from the measured data. The key advantages of
252 this algorithm are that it minimizes the mean square error in the training dataset and is not
253 restricted in a functional linearity form, such as a linear regression model, as long as the
254 function is monotonic increasing (Barlow et al., 1972). Figure 5 illustrates the difference
255 between a linear regression and isotonic regression model. More information about this
256 algorithm was given in Kruskal (1964) and de Leeuw et al. (2009).



257

258

Fig.1. A comparison between an Isotonic Regression and a linear regression

259

2.5.2. *Sequential Minimal Optimization Regression (SMOR)*

260

Sequential Minimal Optimization Regression (SMOR) was first introduced by Platt (1999)

261

and later improved by Smola and Schölkopf (1998) and Shevade et al. (2000) for solving

262

very large quadratic programming issues which can occur during the training of a SVM

263

algorithm. These programming issues are divided into a smaller series of optimization

264

quadratic programming sub-issues based on Osuna's theorem (Osuna et al., 1997). Next, an

265

objective function is decreased at each step until a feasible point that satisfies all of the

266

constraints is retained (Yang et al., 2007). The SMOR computes the maximum error

267

deviation (*MED*) between measured and predicted values; if predicted values are higher than

268

MED, performance of the system components was fully satisfactory, and if predicted values

269

are lesser than *MED* the model is often-overlooked (Gao et al. 2019). More information about

270

this algorithm structure can be found in Platt (1999), Yang et al. (2007), Cheng and Qu

271

(2013) and Yang et al. (2014).

272

2.5.3. *Locally Weighted Learning (LWL)*

273

Locally weighted learning (LWL) is a class of function approximation techniques, in which a

274

prediction is made by using an approximated local model around a point of interest. This

275

approximation is achieved by using an instance-based algorithm to assign instance weights

276 which are then used by a specified Weighted Instances Handler. LWL can perform
277 classification (e.g. using naive Bayes) or regression (e.g. using linear regression), and is one
278 of the most widely used lazy learner algorithms. LWL is a simple but appealing tool, both
279 instinctively and statistically, for learning process dynamics of non-linear problems, due to its
280 high flexibility. The main drawback of this algorithm is the longer time required in the
281 modeling process, from model building to making predictions.

282 The algorithm is based on the following equation: if $y(r) = z(x(r), u(r))$ is considered as a
283 non-linear event, the optimum output $u_d(r)$ can be calculated using the inverse approach of
284 the event as follows (Arif et al., 2001):

$$285 \quad u_d(r) = z^{-1}(x_d(r), y_d(r)) \quad (5)$$

286 where $z(\cdot)$ is considered as a non-linear function, $x_d(r)$ are the states, and $y_d(r)$ is the
287 optimum output. More information about this algorithm can be found in Atkeson et al.
288 (1997).

289 **2.5.4. Iterative Classifier Optimizer (ICO)**

290 The Iterative Classifier Optimizer (ICO) algorithm uses a cross-validation or percentage split
291 approach to optimize the number of iterations of the given iterative classifier. The algorithm
292 has the ability to handle missing, nominal, binary classes and attributes like numeric,
293 nominal, binary and empty nominal (Saad, 2018). A two iteration process is used: models are
294 run and the results compared with measured values and then feedback is submitted to the
295 model to further learn and fine tune the results.

296 **2.5.5. Least Median of Squares Regression (LMS)**

297 The Least Median of Squares Regression (LMS) algorithm implements a least median
298 squared linear regression using the existing (weka) linear regression class to form predictions.

299 These LMS functions are generated from random subsamples of the data. The LMS with the
300 lowest median squared error is chosen as the final model. More information about this
301 algorithm is presented in Rousseeuw and Leroy (1987) and Giloni (2002).

302 **2.5.6. Disjoint Aggregating (Dagging)**

303 The Disjoint Aggregating (DA) algorithm is a type of meta-classifier that creates a number of
304 disjoint, stratified folds out of the data and feeds each chunk of data to a copy of the supplied
305 base classifier. Predictions are made via averaging, since all the generated base classifiers are
306 put into the Vote Meta classifier. The algorithm is useful for base classifiers that are quadratic
307 or worse in time behavior, in regard to the number of instances in the training data. The
308 strong capabilities of this algorithm include handling missing class values, binary class,
309 nominal class, nominal attributes, empty nominal attributes and unary attributes. More
310 information about this algorithm can be found in Ting and Witten (1997).

311 **2.5.7. Random Subspace**

312 Random Subspace (RS) constructs a decision tree based classifier that maintains the highest
313 accuracy on the training data and improves generalization accuracy as it grows in complexity
314 (Ho, 1998). This algorithm enhances the prediction power of the weak classifier algorithms.
315 The classifier in this algorithm consists of multiple trees constructed systematically by
316 pseudo randomly selecting subsets of components of the feature vector, that is, trees
317 constructed in randomly chosen subspaces. More information about this algorithm can be
318 found in Ho (1998).

319 **2.6. Model evaluation**

320 After the determination of the most effective input variable combination and the optimum
321 operator values, each algorithm was trained by a training dataset and evaluated by a testing
322 dataset. Since the models were built by a training dataset, this evaluation can only show how

323 well the constructed model fits the testing dataset, and cannot be used for model validation
 324 (Chen et al., 2019). For a visual analysis and assessment of the applied models, scatter plots,
 325 Taylor diagrams and box-plots were used. One distinct advantage of the Taylor diagram is
 326 that it benefits from the use of the two most common correlation statistics: correlation and
 327 standard deviation (*SD*) (Taylor, 2001). Points are depicted on the diagram to compare the
 328 performance of different developed models. The measured data point in the Taylor diagram is
 329 considered as the reference point. The closer the predicted value to this reference value, in
 330 terms of *r* and *SD*, the higher the prediction capability. The advantage of a box-plot is that it
 331 can show how well a model predicts extreme, median and quartile values.

332

333 In addition, *RMSE*, Mean Absolute Error (*MAE*), the Nash-Sutcliffe efficiency (*NSE*) were
 334 used to quantify model performance. These criteria were calculated as follows:

$$335 \quad RMSE = \sqrt{\frac{1}{N} \sum_{i=1}^N [(d_{sm}/b_1)_i - (d_{sp}/b_1)_i]^2} \quad (6)$$

336

$$337 \quad MAE = \frac{1}{N} \sum_{i=1}^N |(d_{sm}/b_1)_i - (d_{sp}/b_1)_i| \quad (7)$$

338

$$339 \quad NSE = 1 - \frac{\sum_{i=1}^N [(d_{sm}/b_1)_i - (d_{sp}/b_1)_i]^2}{\sum_{i=1}^N [(d_{sm}/b_1)_i - \overline{d_{sm}}/b_1]^2} \quad (8)$$

340

341 where $d_s b_1$ is the scour depth, *N* is the number of datasets, $\overline{d_s}/b_1$ is the mean scour depth, and
 342 *m* and *p* subscripts denote the measured and predicted values, respectively.

343 The lower the *RMSE* and *MAE*, the better the model performance. Model performance can be
 344 classified using the *NSE* values (between $-\infty$ and 1; Moriasi et al., 2007): (i) unsatisfactory:

345 NSE \leq 0.4; (ii) acceptable: 0.40<NSE \leq 0.50; (iii) satisfactory: 0.50<NSE \leq 0.65; (iv) good:
 346 0.65< NSE \leq 0.75; (v) very good: 0.75< NSE \leq 1.00.

347 A reliability analysis was also applied to reveal the consistency of applied models or
 348 permissible level of model performance, as follows:

$$349 \text{ Reliability} = [(1/N) * \sum_{i=1}^N k_i] * 100 \quad (9)$$

350 The variable k_i was estimated based on the relative average error (RAE). If RAE is ≤ 0.2 , then
 351 $k_i = 1$, else $k_i = 0$. This threshold of 0.2 was determined based on the Chinese Standard value
 352 (Saberi-Movahed et al. 2020). RAE was calculated as follows:

$$353 RAE = \left| \frac{(d_{s_m} / b_1) - (d_{s_p} / b_1)}{(d_{s_m} / b_1)} \right| \quad (10)$$

354

355 **3. Results and analysis**

356 **3.1. Most/least effective variables**

357 Table 2 reveals which input parameters had the most effect on local scour depth. According
 358 to the correlation coefficients, Fr_0 had the most impact ($r = -0.62$) followed by b_2/b_1 ($r = -$
 359 0.58), h_1/b_1 ($r = -0.56$), σ_g ($r = 0.34$), U_1/U_c ($r = 0.33$), and d_{50}/b_1 ($r = 0.29$).

360 **3.2. Best input combination**

361 Most of the algorithms performed best when all the input parameters were involved in the
 362 building of the model (input No. 6). In six scenarios, this was not the case, and input
 363 combinations 3, 4 and 5 gave the lowest $RMSE$ values correlation coefficients between
 364 observed and predicted scour depth. This contrast reflects the different structures of the
 365 algorithms.

366 A comparison in r values between combinations 1 and 2 shows that adding the b_2/b_1
367 parameter caused the prediction accuracy to significantly decrease for the majority of
368 algorithms. In contrast, adding the h_1/b_1 parameter enhanced the prediction performance of all
369 algorithms significantly (comparison between input No. 2 and 3). The effect of adding σ_g
370 was more mixed, causing an increase in some cases, and little change in others (see the
371 comparison between No. 3 and No. 4). Adding U_1/U_c and d_{50}/b_1 caused the model
372 performance to improve in the majority of cases.

373

374 The models with just one or two input parameters failed to provide accurate predictions of
375 scour depth. This poor performance occurred because some parameters had a poor linear
376 correlation with d_s/b_1 , since the correlation was non-linear. However incorporating these
377 parameters into the models that can handle non-linear relationships enhanced the model
378 accuracy significantly.

379

380 **3.3. Models performance evaluation**

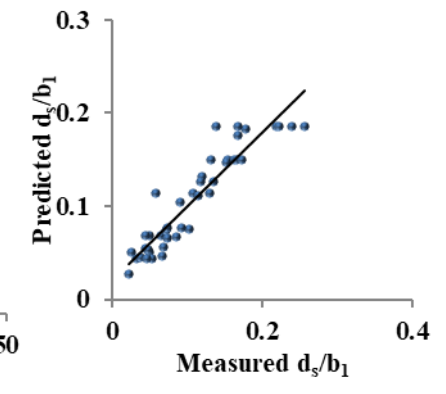
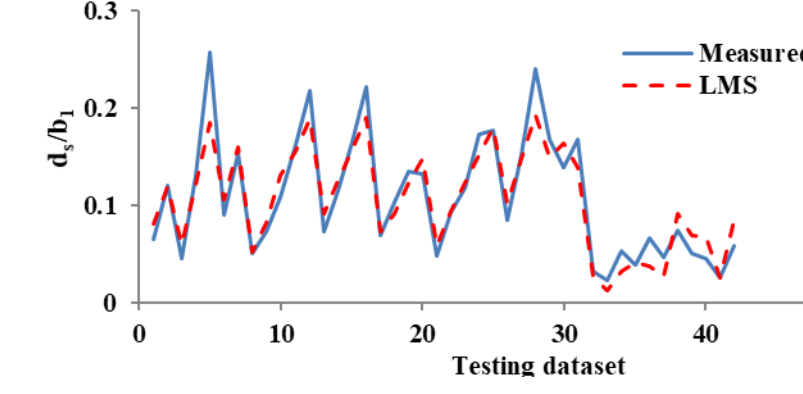
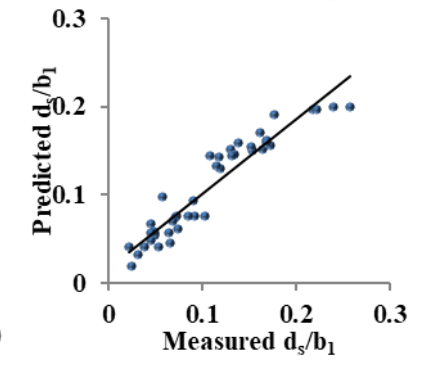
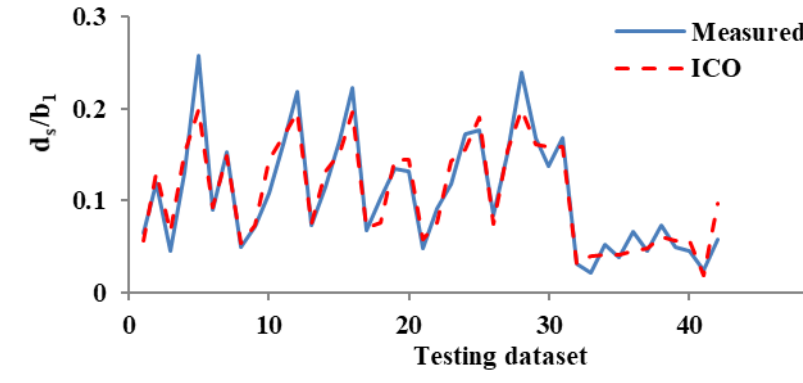
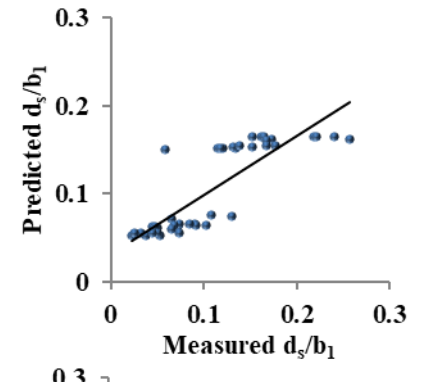
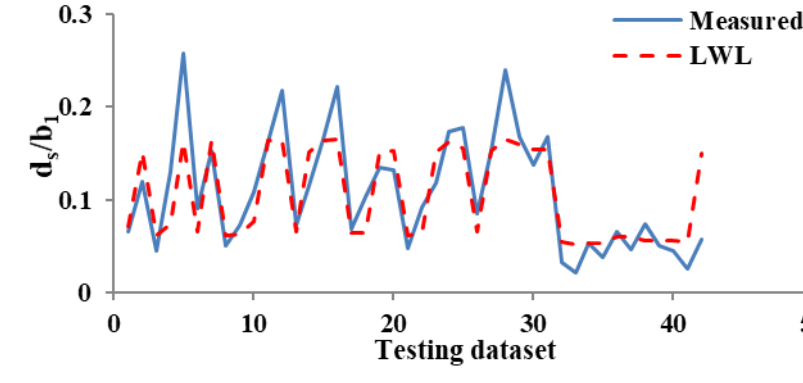
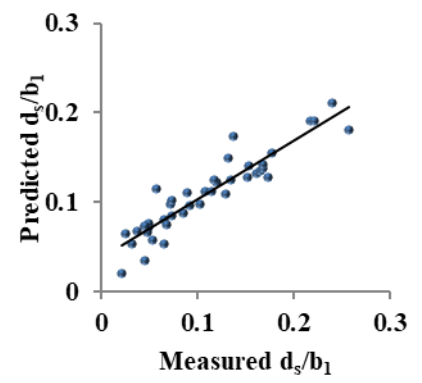
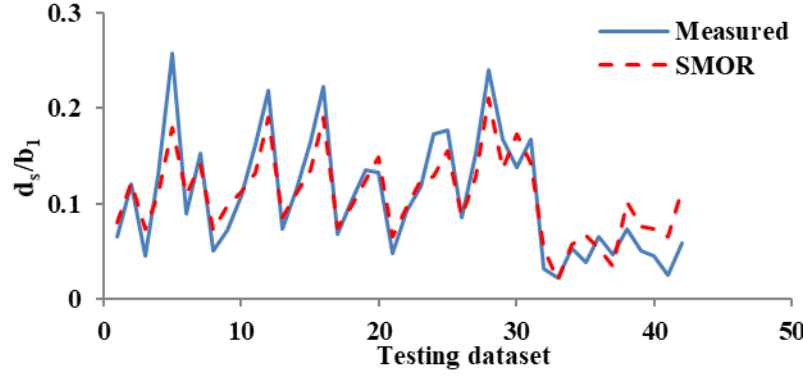
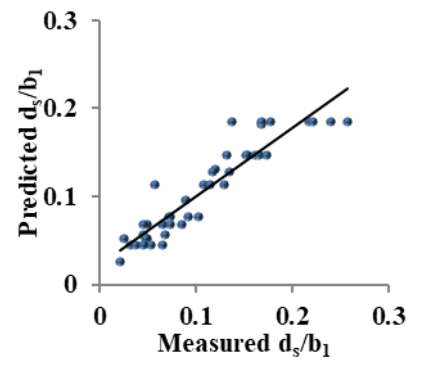
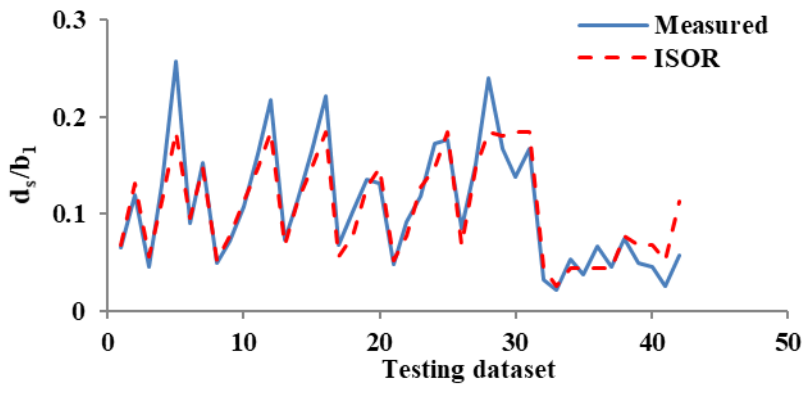
381 A visual comparison of the prediction power of the machine learning models is shown in
382 Figure 2. These plots reveal that all developed algorithms could predict scour depth
383 reasonably well, but all algorithms underestimated the maximum scour depth, except DA-
384 ICO which predicted scour depth almost perfectly. The LWL algorithm by contrast had the
385 weakest performance. Among the standalone algorithms, the ICO model provided slightly
386 better performance than others.

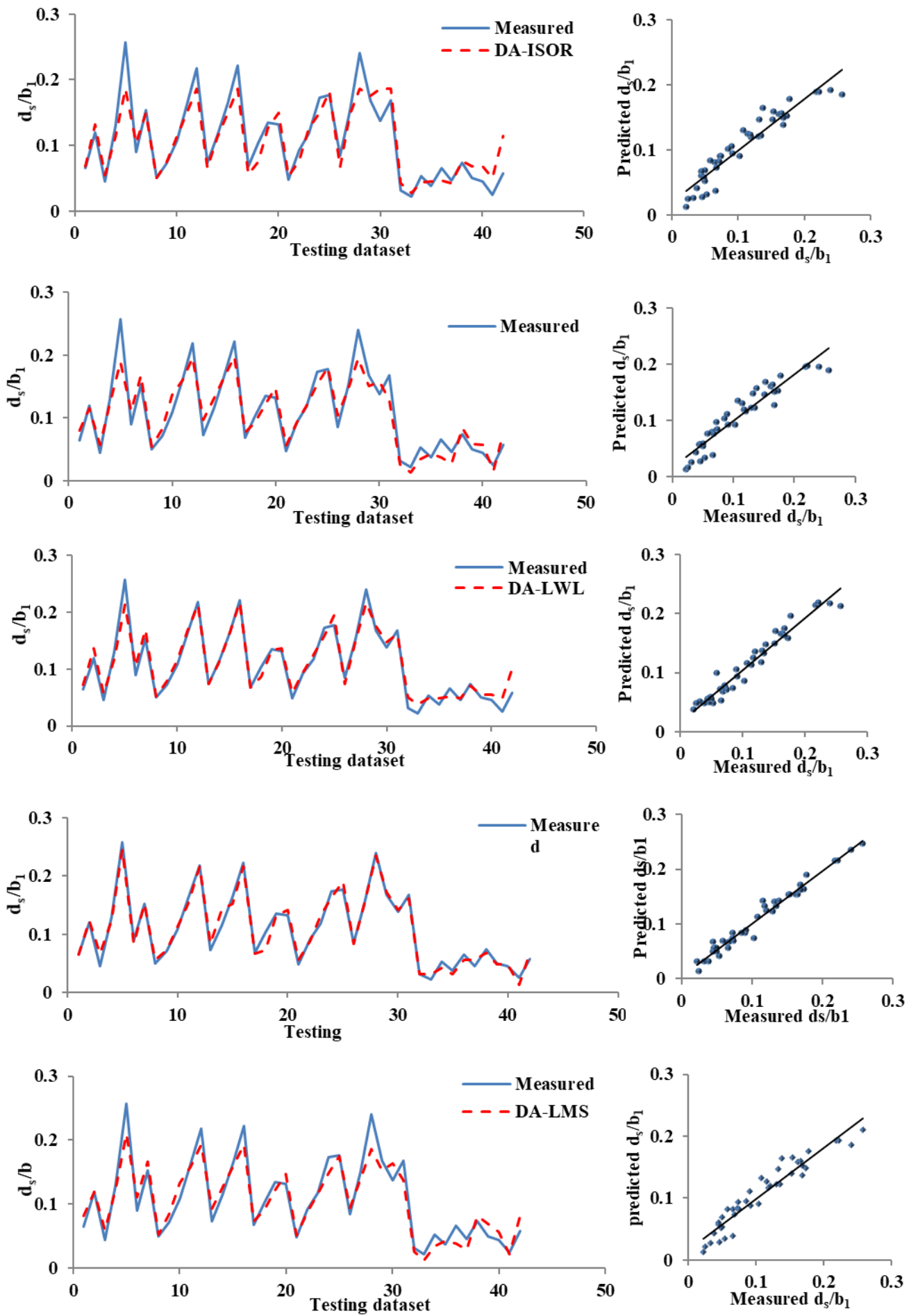
387

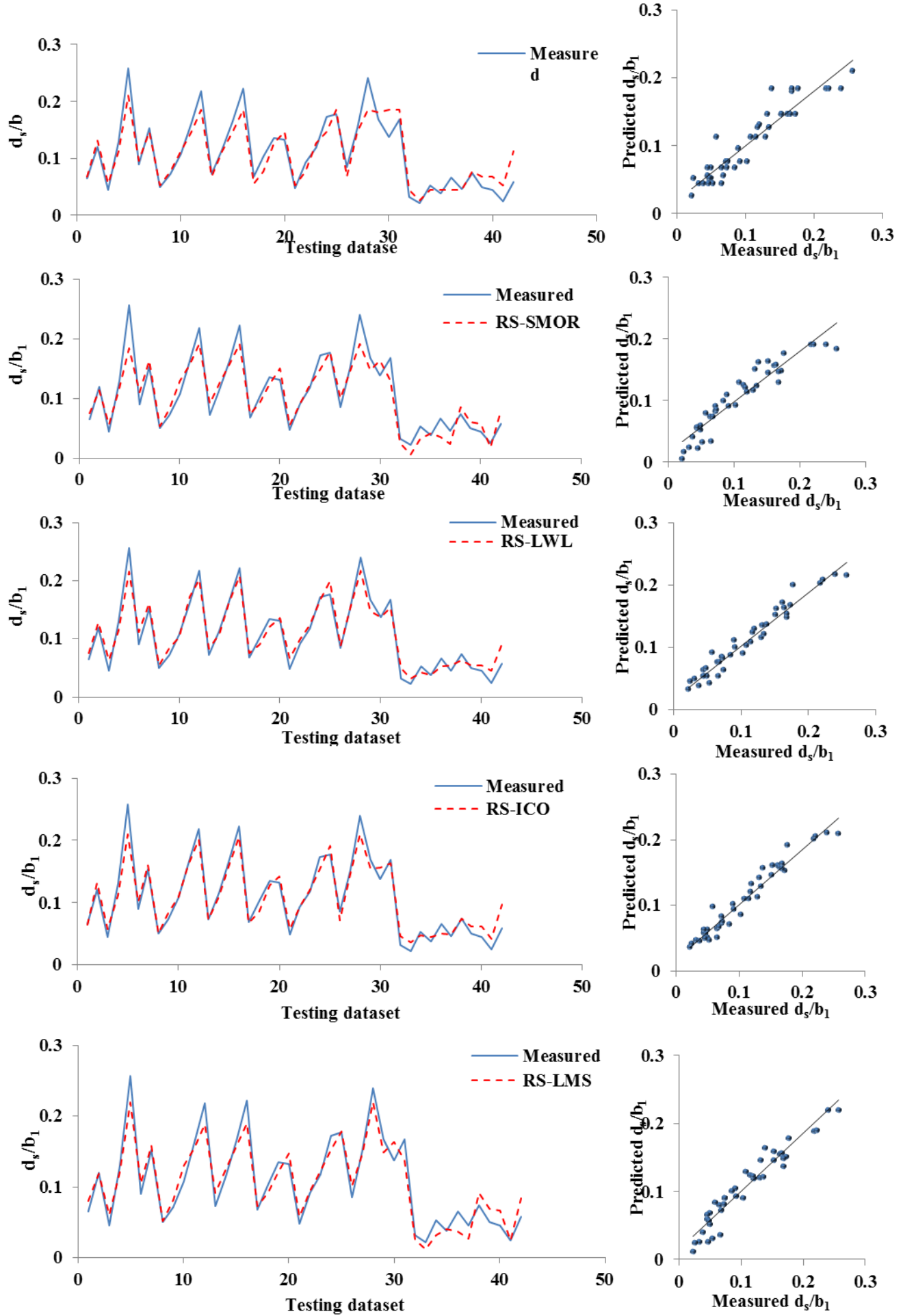
388 Table 4. Correlation coefficient values of model performance for different input combinations

Models	Input number.											
	1		2		3		4		5		6	
	Training	Testing	Training	Testing	Training	Testing	Training	Testing	Training	Testing	Training	Testing
ISO	0.92	0.928	0.92	0.929	0.92	0.929	0.902	0.93	0.92	0.933	0.902	0.935
SMO	0.6	0.8	0.68	0.74	0.85	0.905	0.83	0.88	0.912	0.944	0.913	0.945
LWL	0.82	0.81	0.83	0.82	0.86	0.849	0.856	0.843	0.858	0.844	0.862	0.84
ICO	0.9	0.9	0.92	0.91	0.934	0.93	0.943	0.946	0.938	0.927	0.936	0.92
LMS	0.6	0.8	0.684	0.742	0.81	0.865	0.81	0.865	0.815	0.865	0.836	0.881
DA-ISO	0.92	0.931	0.916	0.93	0.916	0.93	0.916	0.934	0.916	0.939	0.916	0.942
DA-SMO	0.61	0.81	0.68	0.75	0.84	0.898	0.834	0.889	0.913	0.948	0.914	0.951
DA-LWL	0.86	0.87	0.87	0.87	0.88	0.87	0.887	0.875	0.891	0.886	0.892	0.896
DA-ICO	0.91	0.928	0.93	0.94	0.942	0.946	0.95	0.95	0.949	0.948	0.949	0.943
DA-LMS	0.6	0.81	0.672	0.777	0.81	0.863	0.81	0.879	0.861	0.918	0.879	0.917
RS-ISO	0.92	0.93	0.844	0.843	0.91	0.93	0.919	0.93	0.866	0.866	0.934	0.94
RS-SMO	0.6	0.8	0.68	0.707	0.76	0.88	0.752	0.89	0.838	0.935	0.736	0.867
RS-LWL	0.82	0.81	0.83	0.826	0.87	0.87	0.884	0.88	0.876	0.862	0.877	0.874
RS-ICO	0.902	0.904	0.927	0.913	0.941	0.935	0.939	0.931	0.946	0.945	0.949	0.951
RS-LMS	0.600	0.800	0.684	0.746	0.810	0.865	0.810	0.865	0.815	0.865	0.836	0.881

389 * Shadow cells show optimum input number

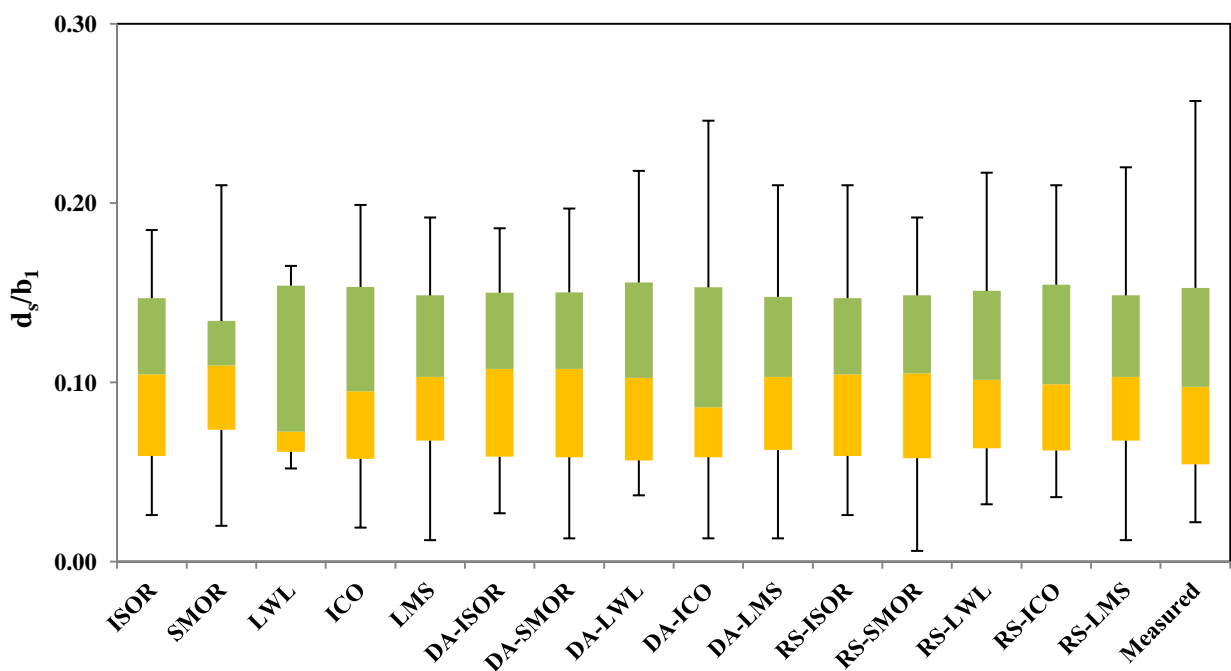






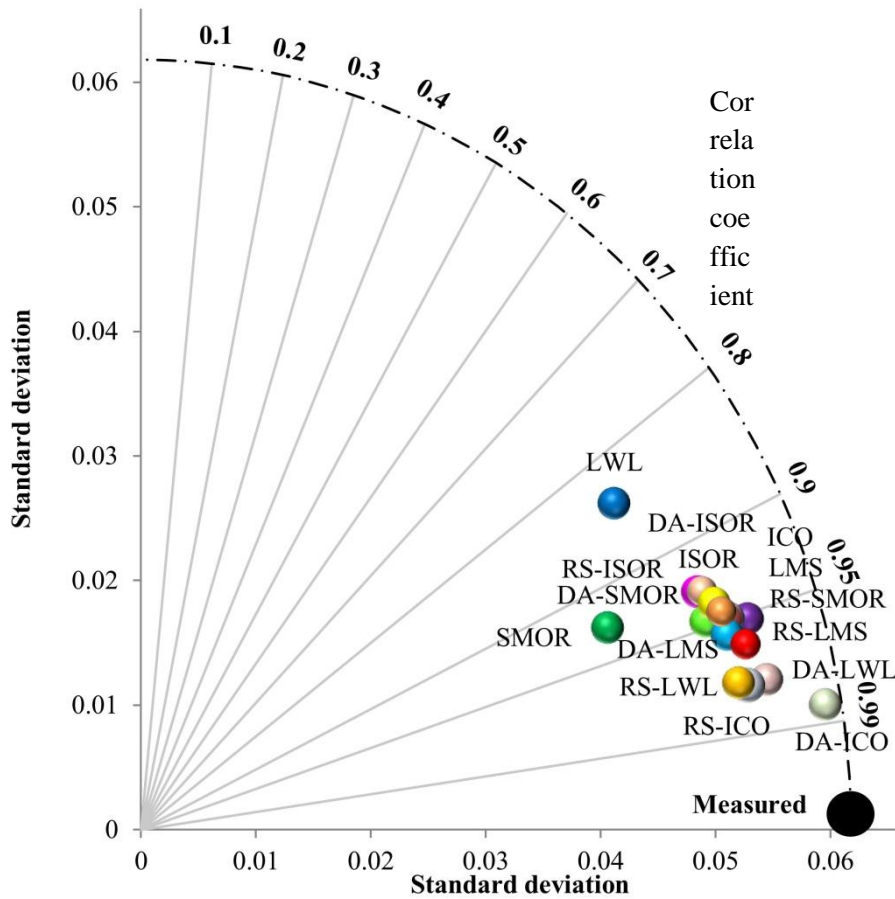
392 Fig 2. Comparison between predicted and measured d_s/b_1 values during the testing phase.

393 To further compare the performance of the standalone and hybridized machine learning
 394 models, box-plots are shown in Figure 3. Only the DA-ICO model predicted maximum scour
 395 depth well (but not perfectly) and all other algorithms underestimated maximum values. The
 396 SMOR and ICO models estimated minimum scour depth very well. The first quartile value
 397 was very well replicated by the DA-LWL model, and ICO, DA-ICO and RS-ICO models
 398 predicted the third quartile most accurately. The RS-ICO model estimated the median scour
 399 depth almost perfectly.



400
 401 Fig. 3. Box plots of observed and predicted d_s/b_1 .
 402

403 The DA-ICO model was closest to the observed reference point in the Taylor plot (Figure 4).
 404 This plot showed that the DA-ICO model had the highest performance because the predicted
 405 standard deviation of scour depth was closest to the standard deviation of the observed data,
 406 and the correlation was also the highest. The DA-LWL, RS-LWL and RS-ICO points almost
 407 overlapped on each other on the Taylor plot, indicating similar model performance.



408

409

Fig.4. Taylor plot of model performance

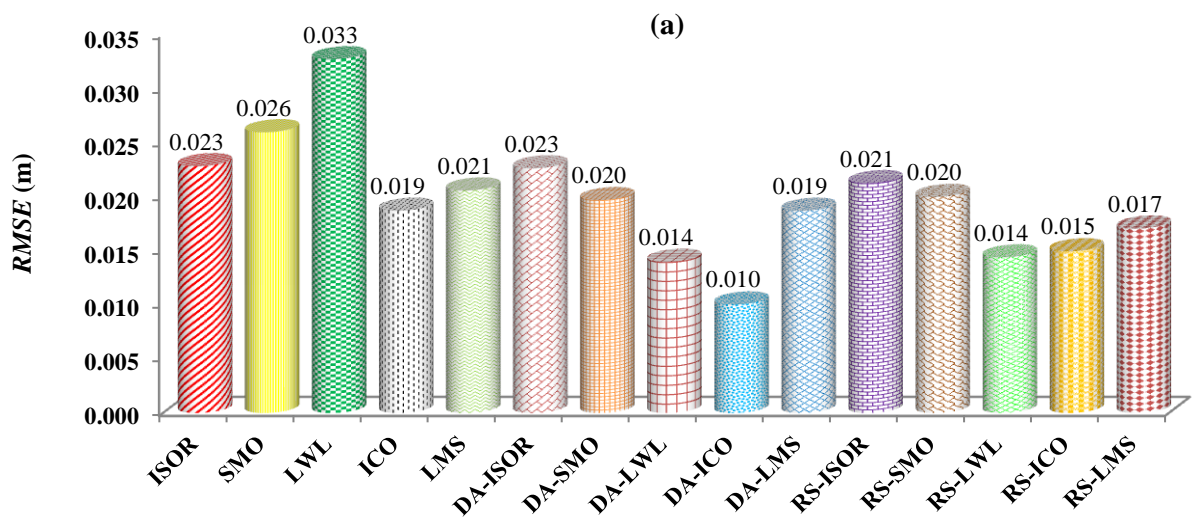
410

411 A quantitative assessment of the predictive capability of the developed models is shown in
 412 Figure 5. Looking across all the evaluation metrics, the DA-ICO model provided the
 413 strongest performance with *RMSE*, *MAE* and *NSE* values of 0.010 m, 0.008 m and 0.972,
 414 respectively. The next strongest performing model was DA-LWL, followed by RS-LWL, RS-
 415 ICO, RS-LMS, DA-LMS=ICO, DA-SMOR=RS-SMOR, RS-ISOR=LMS, DA-ISOR=ISOR,
 416 SMOR and LWL. According to the *NSE* metric, all the developed algorithms had a ‘very
 417 good’ prediction power except the LWL model, which had ‘good’ performance.

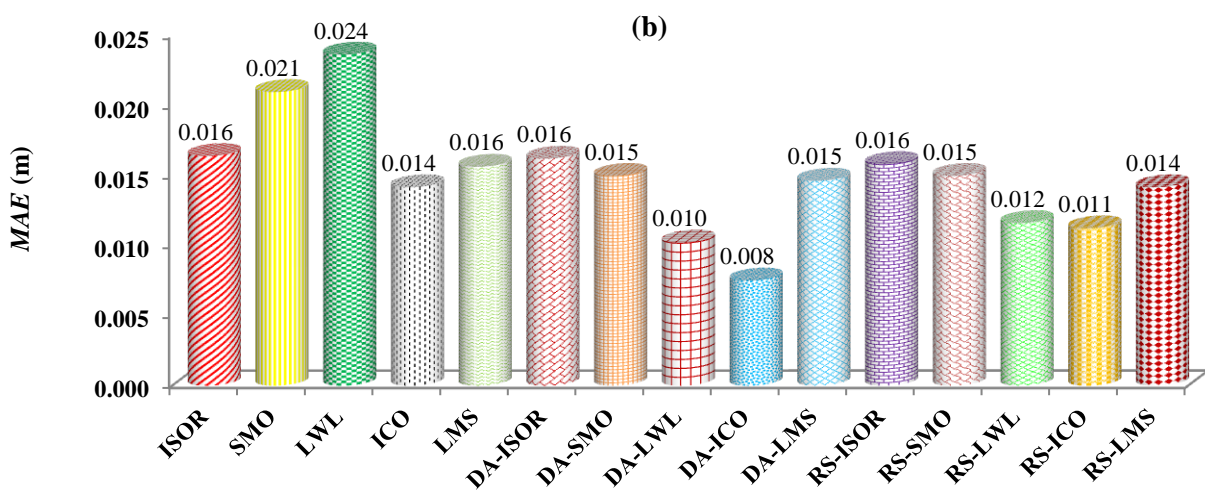
418 The standalone LWL and SMO models gave the lowest performance with higher *RMSE* and
 419 *MAE*, and low *NSE* values. Among the standalone models, ICO produced the most accurate

420 predictions. All the metrics reveal the hybridized version of the machine learning algorithm
 421 outperformed the standalone counterpart. For example, the standalone LWL model had a
 422 *RMSE* value of 0.033 m, while the DA-LWL and RS-LWL models produced a *RMSE* value
 423 of 0.014 m. This hybridization represented a 58% improvement in standalone LWL
 424 performance. In terms of *RMSE* values, hybridization with DA and RS algorithms enhanced
 425 the performance of SMOR models by 23%, ICO by 41% (DA) and 21% (RS), LMS models
 426 by 10% (DA) and 19% (RS), and ISOR by 9% (RA). The *RMSE* values were the same for
 427 ISOR and DA-ISOR models.

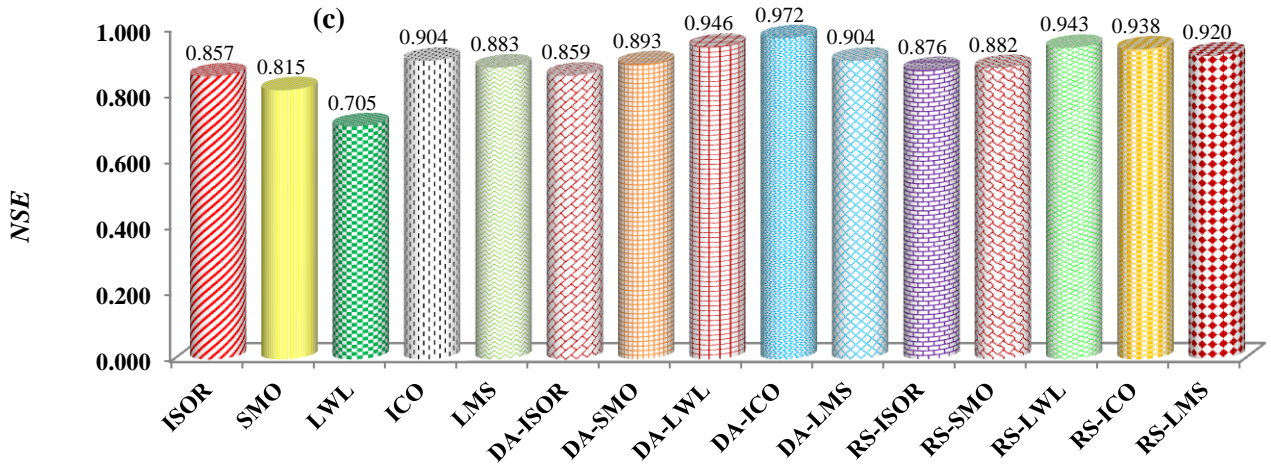
428



429



430



431

432

Fig. 5. Model evaluation using quantitative criteria

433

A Reliability analysis showed that the DA-ICO hybrid model had the highest level of

434

reliability (83.3%), while the standalone model of LWL had the lowest degree of reliability

435

(45.2%). In all but one case (DA-ISOR) hybridization enhanced reliability (Table 5).

436

Table 5. Model reliability.

Model	Reliability (%)
ICO	71.4
ISOR	73.8
LMS	64.3
LWL	45.2
SMOR	59.5
DA-ICO	83.3
DA-ISOR	69.0
DA-LMS	69.0
DA-LWL	78.6
DA-SMOR	64.3
RS-ICO	81.0
RS-ISOR	76.2
RS-LMS	71.4
RS-LWL	81.0
RS-SMOR	69.0

437 **4. Discussion**

438 Scouring takes place in clear water flow due to a contraction resulting from a change in
439 channel cross-section shape. For a given discharge, reducing the channel width causes an
440 increase in flow velocity, bed shear stress and thus scour. In order to compute the scour depth
441 in such a hydraulic condition, several empirical equations have been proposed in the
442 literature, developed using conventional regression analysis. These equations are based on the
443 most important variables considered to affect scour depth, such as channel width, flow depth
444 and velocity in the un-contracted and contracted sections of the channel. These empirical
445 equations do not perform as accurately as machine learning algorithms (Najafzadeh et al.
446 2018). However no study has examined the performance of hybrid machine learning
447 algorithms in predicting scour depth. To this end, this study sought to provide the first
448 comparison of the accuracy of these novel algorithms with standalone machine learning
449 algorithms and empirical equations.

450 The determination of the best input variable combination is one of the most critical steps in
451 producing an accurate machine learning model. Some researchers have determined the best
452 input combination according to the highest correlation coefficient in a multiple regression
453 (Barzegar et al. 2016). However the current paper shows this approach for scour prediction is
454 not the best to take because the best input combination was not the same for all algorithms
455 and, due to nonlinearity between variables, the variables with low correlation coefficients
456 with scour depth enhanced the prediction power of the some of the models. Thus a range of
457 different input variable combinations must be considered in the optimization of machine
458 learning models.

459 In order to find the best input combination, a sensitivity analysis was carried out to
460 investigate the importance of each dimensionless parameter in scour depth computation. The
461 results revealed that upstream, unconstructed densimetric particle Froude number had the

462 greatest impact on scour depth prediction, in accordance to previous laboratory experiments
463 (Li et al., 2002). This result is also consistent with Dey and Raikar (2005) who illustrated that
464 the upstream densimetric particle Froude number had the greatest effect on scour depth, in
465 which an increase in this number decreased the scour depth. This parameter represents the
466 impact of the mobility of submerged sediment particles on scour depth (Dey and Raikar,
467 2005) and has been proposed as suitable for defining the initiation of sediment motion
468 (Aguirre-Pe et al., 2003). Thus it is reasonable to expect the particle Froude number to have
469 this important impact on scour depth. In our study we estimated the densimetric particle
470 Froude number based on the ratio between the approach flow velocity and submerged weight
471 of the sediment. The particle Froude number can also be obtained, when data is available,
472 through analyzing the hydrodynamic forces - lift, drag resistance and submerged weight -
473 acting on the sediment particle in equilibrium conditions (Safari et al., 2017). The drag and
474 lift forces have a positive effect on sediment motion, and the buoyed weight of the sediment
475 and resistance force have the opposite effect. Therefore, to initiate scour, the flow must have
476 adequate force to overcome this buoyed weight and resistance force. An alternative method to
477 estimate the particle Froude number is to combine the Shields sediment threshold equation
478 (1936) with the Manning (1891) flow resistance formula. In this formulation the particle
479 Froude number is an alternative type of Shields (1936) threshold parameter, expressed in
480 terms of velocity rather than shear stress (Safari et al., 2015).

481 The DA-ICO was found to provide the most accurate predictions of scour depth using four
482 input parameters: Fr_0 , b_2/b_1 , h_1/b_1 and σ_g . For most of the other models, six input parameters
483 were required to provide the optimum prediction performance. Thus a further advantage of
484 the DA-ICO is in its relative simplicity, using parameters that are more readily and easily
485 measured, removing the requirement to measure the approach and critical flow velocity. The

486 ISOR, DA-ISOR and RS-ISOR algorithms gave reasonable prediction accuracy with only Fr_0
487 as an input, demonstrating their efficiency.

488 The hybrid models had a higher prediction power than standalone models because hybrid
489 models are more flexible than standalone models and have a nonlinear structure (De'ath and
490 Fabricius, 2000). These two model properties are particularly important in the prediction of
491 scour depth because of the nonlinearity between variables. The LWL algorithm was the worst
492 performing because in the LWL algorithm, fitting the noise data causes a higher prediction
493 error if noise in the dataset is not filtered out well, and the algorithm does not have the ability
494 to interpolate smoothly between datasets (Schneiderm and Moore, 1997).

495 The difference in performance between algorithms is attributable to their different
496 computational structures. The DA-ICO model provided the most accurate predictions for two
497 reasons. First, the ICO algorithm uses a cross-validation or percentage split approach to
498 optimize the number of iterations. Secondly, the Dagging algorithm benefits from ensemble
499 learning in its structure (multiple weak learners) which outperforms a single strong learner
500 (Dietterichm 1997). This learning helps to reduce variance and avoid the over-fitting problem
501 caused by the use of a bootstrap procedure.

502 Najafzadeh et al. (2016, 2018), using the same datasets as the current paper, compared the
503 performance of traditional AI-based algorithms (SVM, ANFIS, GEP, EPR and MT) with the
504 empirical equations of Laursen (1963), Komura (1966), Gill (1981) and Lim (1993). Table 6
505 shows this comparison, along with the current paper's *RMSE* value for the best performing
506 hybrid machine learning algorithm. The table shows that the GEP model (*RMSE* = 0.027 m)
507 outperformed all empirical equations, and the newly developed DA-ICO model (*RMSE* =
508 0.010 m) performed significantly better than the GEP model (a 62% improvement in *RMSE*).
509 When compared to the empirical equations in terms of *RMSE* values, the DA-ICO model had

510 82% (Laursen, 1963), 93% (Lim, 1993), 95% (Komura, 1966) and 99% (Gill, 1981) better
 511 accuracy.

512 Table 6. A comparison of model performance between traditional AI-based algorithms, GEP,
 513 MT and EPR Najafizadeh et al. (2016, 2017), empirical equations (Laursem, 1963; Komura,
 514 1966; Gill, 1981; Lim, 1993) and DA-ICO, the best performing hybrid machine learning
 515 algorithm in the current study.

Model	<i>RMSE</i> (m)	Model	<i>RMSE</i> (m)	Model	<i>RMSE</i> (m)
GEP	0.0260	SVM	0.028	Komura (1966)	0.0833
MT	0.0296	ANFIS	0.0281	Gill (1981)	0.200
EPR	0.0263	Laursen (1963)	0.0543	Lim (1993)	0.134

516

517 Overall, the results show that DA-ICO models have great potential to produce robust
 518 predictions of scour depth in long contractions in clear-water conditions. As well as offering
 519 far superior prediction accuracy than existing empirical and traditional AI-models, a distinct
 520 strength of this model is the need for just four readily measured dimensionless variables:
 521 densimetric particle Froude number, width of the un-contracted section, approach flow depth
 522 and sediment geometric standard deviation. Thus this type of data-driven model could be of
 523 real practical benefit to engineers required to estimate maximum scour depth when designing
 524 bridges, weirs, spur dike and cofferdams. Future studies should consider the performance of
 525 these algorithms in the prediction of scour depth in more complex conditions, such as within
 526 natural rivers, than those featured in the studied datasets, such as, live-bed scour, non-
 527 rectangular channels, unsteady flows, non-equilibrium transport conditions, and water-
 528 worked beds that mimic better the surface topographies of natural coarse-grained rivers
 529 (Cooper and Tait, 2009).

530

531 **5. Conclusion**

532 The accurate prediction of scour depth is vital for preventing the collapse of in-channel
533 structures. Due to the non-linear behavior of sediment transport in a river, hybrid machine
534 learning algorithms have great potential to produce accurate predictions of scour depth in
535 long contractions. Using previously collected scour depth data from laboratory flume
536 experiments, this study tested this potential for the first time by comparing the prediction
537 power of five standalone algorithms, Isotonic Regression (ISOR), Sequential Minimal
538 Optimization (SMO), Iterative Classifier Optimizer (ICO), Locally Weighted learning (LWL)
539 and Least Median of Squares Regression (LMS) and their hybrid versions with Dagging
540 (DA) and Random Subspace (RS) algorithms (i.e., DA-ISOR, DA-SMOR, DA-LWL, DA-
541 ICO, DA-LMS, RS-ISOR, RS-SMOR, RS-LWL, RS-ICO, RS-LMS). The main findings
542 were as follows:

- 543 (1) A test of model performance showed that the DA-ICO model had the highest
544 prediction power followed by DA-LWL, RS-LWL, RS-ICO, RS-LMS, DA-LMS,
545 ICO, DA-SMOR=RS-SMOR, RS-ISOR=LMS, DA-ISOR=ISOR, SMOR and LWL.
546 All models displayed ‘very good’ performance except the LWL model, which had
547 ‘good’ performance.
- 548 (2) The hybrid models had a higher prediction power than standalone models because the
549 hybrid models are more flexible and have a nonlinear structure that better represents
550 the nonlinear behavior of sediment transport.
- 551 (3) All algorithms underestimated the maximum scour depth, except DA-ICO which
552 predicted scour depth almost perfectly.
- 553 (4) A sensitivity analysis revealed that scour depth was most sensitive to the densimetric
554 particle Froude number followed by the non-dimensionalized contraction width, flow

555 depth within the contraction, sediment geometric standard deviation, approach flow
556 velocity and median grain size.

557 (5) Most of the algorithms performed best when all the input parameters were involved in
558 the building of the model. An important exception was the best performing model,
559 which required only four input parameters: densimetric particle Froude number and
560 non-dimensionalized contraction width, flow depth within the contraction and
561 sediment geometric standard deviation.

562 (6) Variables with low correlation coefficients with scour depth enhanced the prediction
563 power of the some of the models. Thus a range of different input variable
564 combinations must be considered in the optimization of machine learning models.

565 Overall the results revealed that hybrid machine learning algorithms provide more accurate
566 predictions of scour depth than empirical equations and traditional AI-algorithms. The DA-
567 ICO model not only created the most accurate predictions but also used the fewest easily and
568 readily measured input parameters. Thus this type of model could be of real benefit to
569 practicing engineers required to estimate maximum scour depth when designing in-channel
570 structures. In this case, understanding more about the potential for hybrid machine learning
571 algorithms to provide relatively cheap and fast predictions of scour depth in more complex
572 hydro-sedimentary conditions represents a vital research avenue.

573

574 **References**

575 Aguirre-Pe J, Olivero ML, Moncada AT (2003) Particle densimetric Froude number for estimating
576 sediment transport. *J Hydraul Eng* 129(6):428–437

577 Ashida, K. 1963. Study on the stable channel through constrictions. Annual Report, Disaster
578 Prevention Research Institute, Kyoto University, Kyoto, Japan, 1-15.

579 Atkeson, C., Moore, A., Schaal, S. 1997. Locally Weighted Learning, *Artificial Intelligence Review*,
580 11:11-73.

581 Ayoubloo, M. K., A. Etemad-Shahidi, and J. Mahjoobi. 2010. Evaluation of regular wave scour
582 around a circular pile using data mining approaches. *Applied Ocean Research* 32 (1), 34–39.
583 doi:10.1016/j.apor.2010.05.003

584 Azamathulla, H. M., A. Ab Ghani, N. A. Zakaria, and A. Guven. 2010. Genetic programming to
585 predict bridge pier scour. *Journal of Hydraulic Engineering, ASCE* 136 (3), 165–69.

586 Azmathullah, H.M., Ghani, A.A.B., Zakaria, N.A., 2009. ANFIS based approach for predicting
587 maximum scour location of spillway. *Water Manag. ICE Lond.* 162(6), 399–407.

588 Barlow, R. E.; Bartholomew, D. J.; Bremner, J. M.; Brunk, H. D. (1972). *Statistical inference under*
589 *order restrictions; the theory and application of isotonic regression.* New York: Wiley. ISBN 978-
590 0-471-04970-8.

591 Bui, A Shirzadi, K Chapi, H Shahabi, B Pradhan, BT Pham, 2019b A hybrid computational
592 intelligence approach to groundwater spring potential mapping. *Water* 11 (10), 2013

593 Bui, D., Khosravi, K., Karimi, M., Khozani, Z., Nguyen, H. et al. 2020b. Enhancing nitrate and
594 strontium concentration prediction in groundwater by using new data mining algorithm. *Science of*
595 *The Total Environment*, 136836

596 Bui, D., Khosravi, K., Tiefenbacher, J., Nguyen, H., Kazakis, N. 2020. Improving prediction of water
597 quality indices using novel hybrid machine-learning algorithms. *Science of The Total*
598 *Environment*, 13761.

599 Bui, D., Pradhan, B., Nampak, H., Bui, Q.-T., Tran, Q.-A., Nguyen, Q.-P., 2016. Hybrid artificial
600 intelligence approach based on neural fuzzy inference model and metaheuristic optimization
601 for flood susceptibility modeling in a high-frequency tropical cyclone area. *Journal of*
602 *hydrology*.

603 Bui, D., Shahabi, H., Omidvar, E., Shirzadi, A., Geertsema, M., Clague, J., Khosravi, K., Pradhan, B.,
604 Pham, B., Chapi, K., Barati, Z., Bin Ahmad, Rahmani, H., Lee, S. 2019a. Shallow landslide
605 prediction using a novel hybrid functional machine learning algorithm. *Remote Sensing*, 11 (8):
606 931

607 Chan-Yun Yang, Kuo-Ho Su and Gene Eu Jan, "An elaboration of sequential minimal optimization
608 for support vector regression," *2014 IEEE International Conference on System Science and
609 Engineering (ICSSE)*, Shanghai, 2014, pp. 88-93

610 Chen, W., Panahi, M., Khosravi, K., Poughasemi, H.R., Rezaei, F. 2019. Spatial prediction of
611 groundwater potentiality using ANFIS ensembled with teaching-learning-based and biogeography-
612 based optimization, *Journal of Hydrology* 572, 435-448

613 Cheng, L., Qu, X. 2013. Advanced Technologies on Measure and Diagnosis, *Manufacturing Systems
614 and Environment Engineering, Applied Mechanics and Materials*, 329:
615 <https://doi.org/10.4028/www.scientific.net/AMM.329.472>

616 Choubin, B., Darabi, H., Rahmati, O., Sajedi-Hosseini, F., Kløve, B., 2018. River suspended
617 sediment modelling using the CART model: A comparative study of machine learning
618 techniques. *Sci. Total Environ.* 615, 272–281. <https://doi.org/10.1016/j.scitotenv.2017.09.293>

619 Cooper, J.R., Tait S.J. 2009. Water-worked gravel beds in laboratory flumes: a natural analogue?
620 *Earth Surface Processes and Landforms.* 34, 384–397, doi: 10.1002/esp.1743D Tien Bui, H
621 Shahabi, E Omidvar, A Shirzadi, M Geertsema, JJ Clague, ...2019a Shallow landslide prediction
622 using a novel hybrid functional machine learning algorithm. *Remote Sensing* 11 (8), 931

623 De Leeuw J, Hornik K, Mair P (2009). "Isotone Optimization in R: Pool-Adjacent-Violators
624 Algorithm (PAVA) and Active Set Methods." *Journal of Statistical Software*, 32(5), 1–24. URL
625 <http://www.jstatsoft.org/v32/i05/>.

626 Dey, S. 1997. "Local scour at piers, part 1: A review of development of research." *Int. J. Sediment
627 Res.*, 122, 23–44.

628 Dey, S., and R. V. Raikar. 2005. Scour in long contractions. *Journal of Hydraulic Engineering, ASCE*
629 131 (12), 1036–49. doi:10.1061/(asce)0733-9429(2005)131:12(1036)

630 Dietterich, T.G. 1997. Machine learning research: Four current directions. *AI Mag.* 18(4), 97–136.

631 Etemad-Shahidi, A., and N. Ghaemi. 2011. Model tree approach for prediction of pile groups
632 scour due to waves. *Ocean Engineering.* 38, 1522–27. doi:10.1016/j.oceaneng.2011.07.012

633 Firat, M. 2009. Scour depth prediction at bridge piers by ANFIS approach. Proceedings of the
634 Institution of Civil Engineers - Water Management, Volume 162 Issue 4, August 2009, pp. 279-
635 288

636 Ghaleh Nou, M. Azhdary Moghaddam, M. Shafai Bajestan, H. Md. Azamathulla; Estimation of scour
637 depth around submerged weirs using self-adaptive extreme learning machine. *Journal of*
638 *Hydroinformatics* 1 November 2019; 21 (6): 1082–1101.
639 doi: <https://doi.org/10.2166/hydro.2019.070>

640 Gi;oni, A., Padberg, M. 20002. Least trimmed squares regression, least median squares regression, and
641 mathematical programming. *Mathematical and Computer Modelling*, 35:1043-1060

642 Gill, M. A. 1981. Bed erosion in rectangular long contraction. *Journal of the Hydraulics Division*
643 *ASCE* 107 (3), 273–84.

644 Guven, A., and M. Gunal. 2008. Genetic programming approach for prediction of local scour
645 downstream hydraulic structures. *Journal of Irrigation and Drainage Engineering*, 134 (2),
646 241–49. doi:10.1061/(asce)0733-9437(2008)134:2(241)

647 Ho, T.K., 1998. The random subspace method for constructing decision forests. *IEEE Trans. Pattern*
648 *Anal. Mach. Intell.* 20, 832–844. <https://doi.org/10.1109/34.709601>

649 K Chapi, VP Singh, A Shirzadi, H Shahabi, DT Bui, BT Pham, K Khosravi. A novel hybrid artificial
650 intelligence approach for flood susceptibility assessment. *Environmental modelling & software* 95,
651 229-245

652 Khosravi K, L Mao, O Kisi, ZM Yaseen, S Shahid. 2018a. Quantifying hourly suspended sediment
653 load using data mining models: case study of a glacierized Andean catchment in Chile. *Journal of*
654 *Hydrology* 567, 165-179

655 Khosravi, K., Pham, B.T., Chapi, K., Shirzadi, A., Shahabi, H., Revhaug, I., Prakash, I., Tien
656 Bui, D., 2018a. A comparative assessment of decision trees algorithms for flash flood
657 susceptibility modeling at Haraz watershed, northern Iran. *Sci. Total Environ.*
658 <https://doi.org/10.1016/j.scitotenv.2018.01.266>

659 Khosravi, K., Barzegar R, Miraki S, Adamowski J, Daggupati P, Pham, B. 2020b. Stochastic
660 Modeling of Groundwater Fluoride Contamination: Introducing Lazy Learners, Groundwater. In
661 press.

662 Khosravi, K., Cooper, J.R., Daggupati, P., Pham, B., Bui, D.T. 2020a. Bedload transport rate
663 prediction: Application of novel hybrid data mining techniques. Journal of Hydrology, 124774. In
664 press. <https://doi.org/10.1016/j.jhydrol.2020.124774>

665 Khosravi, K., Daggupati P, Alami MT, Awadh SM, Ghareb MI, Panahi M, et al. 2019. Meteorological
666 data mining and hybrid data-intelligence models for reference evaporation simulation: A case
667 study in Iraq. Computers and Electronics in Agriculture 167, 105041

668 Khozani, Z., Khosravi, K., Pham, B. T., Kløve, B., Wan Mohtar, W. H. M. & Yaseen, Z. M. 2019.
669 Determination of compound channel apparent shear stress: application of novel data mining
670 models. Journal of Hydroinformatics, doi:10.2166/hydro.2019.037

671 Kisi, O., Ozkan, C., Akay, B., 2012b. Modeling discharge-sediment relationship using neural
672 networks with artificial bee colony algorithm. J. Hydrol. 428–429, 94–103.
673 <https://doi.org/10.1016/j.jhydrol.2012.01.026>

674 Komura, S. 1966. Equilibrium depth of scour in long constrictions. Journal of the Hydraulics
675 Division ASCE 92 (5), 17–38.

676 Komura, S. (1966). Equilibrium depth of scour in long constrictions."J. Hydr. Div., ASCE, 92(5),
677 17-37.

678 Kruskal, J. B. 1964. Nonmetric Multidimensional Scaling: A numerical
679 method. Psychometrika. 29 (2): 115–129. doi:10.1007/BF02289694.

680 Laursen, E. M. 1963. An analysis of relief bridge scour. Journal of the Hydraulics Division ASCE
681 89 (3), 93–118.

682 Laursen, E. M. (1960). Scour at bridge crossing. J. Hydr. Div., ASCE, 86(2), 39-54.

683 Legates, D.R., McCabe, G.J., 1999. Evaluating the use of “goodness-of-fit” measures in
684 hydrologic and hydroclimatic model validation. water Resour. Res. 35, 233–241.

685 Lim, S. Y. 1993. Clear water scour in long contractions. Proceeding of the Institution Civil
686 Engineerings-Waters, Maritime and Energy, London, UK 101 (6), 93–98.

687 Lim, S. Y., and Cheng, N. S. 1998. Scouring in long contractions. *Journal of Irrigation and Drainage*
688 *Engineering ASCE* 124 (5), 258–61. doi:10.1061/(asce)07339437(1998)124:5(258)

689 Maier, H.R., Kapelan, Z., Kasprzyk, J., Kollat, J., Matott, L.S., Cunha, M.C., Dandy, G.C., Gibbs,
690 M.S., Keedwell, E., Marchi, A., Ostfeld, A., Savic, D., Solomatine, D.P., Vrugt, J.A., Zecchin,
691 A.C., Minsker, B.S., Barbour, E.J., Kuczera, G., Pasha, F., Castelletti, A., Giuliani, M., Reed,
692 P.M., 2014. Evolutionary algorithms and other metaheuristics in water resources: current status,
693 research challenges and future directions. *Environ. Modell. Software* 62, 271–299.
694 <https://doi.org/10.1016/j.envsoft.2014.09.013>

695 Manning, R. (1891). "On the flow of water in open channels and pipes". *Transactions of the*
696 *Institution of Civil Engineers of Ireland*. 20: 161–207.

697 Melesse, A.M., Ahmad S, McClain ME, Wang X, Lim YH. 2011. Suspended sediment load
698 prediction of river systems: An artificial neural network approach. *Agricultural Water*
699 *Management* 98 (5), 855-866

700 Moriasi, D.N., Arnold, J.G., Van Liew, M.W., Binger, R.L., Harmel, R.D., Veith, T.L., 2007.
701 Model evaluation guidelines for systematic quantification of accuracy in watershed
702 simulations. *Trans. ASABE* 50, 885–900. <https://doi.org/10.13031/2013.23153>

703 Moussa, Y.A. 2013. Modeling of local scour depth downstream hydraulic structures in trapezoidal
704 channel using GEP and ANNs. *Ain Shams Engineering Journal*, 4:717-722.

705 Muzzammil, M. 2008. Application of Neural Networks To Scour Depth Prediction at The Bridge
706 Abutments, *Engineering Applications of Computational Fluid Mechanics*, 2:1, 30-40,
707 DOI:10.1080/19942060.2008.11015209

708 Najafzadeh, M., A. Etemad-Shahidi, and S.-Y. Lim. 2016. Prediction of scour depth in long
709 contractions using ANFIS and SVM. *Ocean Engineering*, Elsevier 111, 128–35.

710 Najafzadeh, m., Shiri, J., Rezaei Balf, M. 2018. New Expressions-Based Models to Estimate Scour
711 Depth at Clear Water Conditions in Rectangular Channels. *Marine Georesources & Geotechnology*,
712 <http://dx.doi.org/10.1080/1064119X.2017.1303009>

713 Najafzadeh, M., G. A. Barani, and H. M. Azamathulla. 2013. GMDH to prediction of scour
714 depth around vertical piers in cohesive soils. *Applied Ocean Research* 40, 35–41.
715 doi:10.1016/j.apor.2012.12.004

716 Najafzadeh, M., G. A. Barani, and M. R. Hessami-Kermani. 2014. Estimation of pipeline scour due
717 to waves by the group method of data handling. *Journal of Pipeline Systems Engineering*
718 and Practice, ASCE 5 (3), 06014002. doi:10.1061/(asce)ps.1949-1204.0000171

719 Najafzadeh, M., Saberi-Movahed, F. 2019. GMDH-GEP to predict free span expansion rates below
720 pipelines under waves. *Marine Georesources & Geotechnology*, 37(3), 375-392.

721 Onen, F. 2014. Prediction of Scour at a Side-Weir with GEP, ANN and Regression Models. *Arabian*
722 *Journal for Science and Engineering*, 39:6031-6041.

723 Osuna, E. and Freund, R. "An Improved Training Algorithm for Support Vector Machines",
724 *Proceeding of the 1997 IEEE Workshop on Neural Network for Signal Processing*, New York:
725 IEEE, 1997, pp. 276-285.

726 Pal, M., Singh, N.K., Tiwari, N.K., 2014. Kernel methods for pier scour modeling using field data. *J.*
727 *Hydroinf.* 16 (4), 784–796.

728 Parsaie, A., Haghiabi, A.H. & Moradinejad, A. 2019. Prediction of Scour Depth below River Pipeline
729 using Support Vector Machine. *KSCE J Civ Eng* 23, 2503–2513. [https://doi.org/10.1007/s12205-](https://doi.org/10.1007/s12205-019-1327-0)
730 [019-1327-0](https://doi.org/10.1007/s12205-019-1327-0)

731 Pham, B., Prakash, I., Khosravi, K., Chapi, K., Trinh, T., Ngo, T., Hosseini, V., Bui, D. 2019. A
732 comparison of Support Vector Machines and Bayesian algorithms for landslide susceptibility
733 modelling. *Geocarto international*, 34 (13): 1385-1407

734 Platt JC. 1999. Fast training of support vector machines using sequential minimal optimization. In
735 *Advances in Kernel Methods: Support Vector Machines*, Schölkopf B, Burges C, Smola AJ (eds).
736 MIT press: Cambridge, MA; 185–208.

737 Rady, R. 2020. Prediction of local scour around bridge piers: artificial-intelligence-based modeling
738 versus conventional regression methods. *Appl Water Sci* 10, 57. [https://doi.org/10.1007/s13201-](https://doi.org/10.1007/s13201-020-1140-4)
739 [020-1140-4](https://doi.org/10.1007/s13201-020-1140-4)

740 Raikar, R. V. 2004. Local and general scour of gravel beds. PhD thesis, Dept. of Civil
741 Engineering, Indian Institute of Technology, Kharagpur, India.

742 Rousseeuw, P., Leory, A. 1987. Robust regression and outlier detection. Wiley Series in Probability
743 and Statistics, |DOI:10.1002/0471725382

744 Saad, A. 2018. An Efficient Classification Algorithms for Image Retrieval Based Color and Texture
745 Features Iman. Journal of AL-Qadisiyah for computer science and mathematics, 10:42 – 53

746 Saberi-Movahed, F., Najafzadeh, M., Mehrpooya, A. 2020. Receiving More Accurate Predictions for
747 Longitudinal Dispersion Coefficients in Water Pipelines: Training Group Method of Data
748 Handling Using Extreme Learning Machine Conceptions. Water resources management. 34:529–
749 561. <https://doi.org/10.1007/s11269-019-02463-w>

750 Safari, M. J. S., Aksoy, H., Mohammadi, M. 2015. Incipient deposition of sediment in rigid boundary
751 open channels. Environmental Fluid Mechanics, 15(5), 1053-1068.

752 Safari, M. J. S., Aksoy, H., Unal, N. E., Mohammadi, M. 2017. Experimental analysis of sediment
753 incipient motion in rigid boundary open channels. Environmental Fluid Mechanics, 17(6), 1281-1298.

754 Shields, A. 1936. Application of similarity principles and turbulence research to bed-load movement.
755 Preussiischen Research Institute of Hydraulic Engineering, Berlin, Germany, Issue 26.

756 Salih, SQ, Sharafati, A, Khosravi, K, Faris, H, Kisi, O, Tao H, M Ali, Yaseen ZM. 2019. River
757 suspended sediment load prediction based on river discharge information: application of newly
758 developed data mining models. Hydrological Sciences Journal. Under press.

759 Schneidern J., Moore, A. 1997. A Locally Weighted Learning Tutorial using Vizier 1.0

760 Sharafati, A., Khosravi, K., Khosravinia, P., Ahmed, K., Salman, S.A., Mundher, Z., Shamsuddin, Y.,
761 2019. The potential of novel data mining models for global solar radiation prediction. Int. J.
762 Environ. Sci. Technol. <https://doi.org/10.1007/s13762-019-023440>

763 Shevade, S. K., Keerthi, S. S., Bhattacharyya, C., & Murthy, K. R. K. (2000). Improvements to the
764 SMO algorithms for SVM regression. IEEE Transactions on Neural Networks, 11:5, 1188–1193.

765 Smola A.J. and Schölkopf B. 1998a. On a kernel-based method for pattern recognition, regression,
766 approximation and operator inversion. *Algorithmica*, 22: 211–231.

767 Straub, L. G. 1934. Effect of channel contraction works upon regimen of movable bed streams.
768 *Transactions, American Geophysical Union* 2, 454–463. doi:10.1029/tr015i002p00454

769 Taylor, K.E., 2001. Summarizing multiple aspects of model performance in a single diagram. *J.*
770 *Geophys. Res. Atmos.* 106, 7183–7192. <https://doi.org/10.1029/2000JD900719>

771 Tin Kam Ho (1998). The Random Subspace Method for Constructing Decision Forests. *IEEE*
772 *Transactions on Pattern Analysis and Machine Intelligence.* 20(8):832-844. URL
773 <http://citeseer.ist.psu.edu/ho98random.html>.

774 Ting, K. M., Witten, I. H.: Stacking Bagged and Dagged Models. In: Fourteenth international
775 Conference on Machine Learning, San Francisco, CA, 367-375, 1997.

776 Ting, K.M., Witten, I.H., 1997. Stacking bagged and dagged models. (Working paper 97/09).
777 University of Waikato, Department of Computer Science, Hamilton, New Zealand.

778 Webby, M. G. 1984. General scour at contraction. *RRU Bulletin 73*, National Roads Board,
779 Bridge Design and Research Seminar, New Zealand, 109-118.

780 Yang, J. F., Zhai, Y. J., Xu, D. P., & Han, P. (2007). SMO algorithm applied in time series model
781 building and forecast. In 2007 International Conference on Machine Learning and
782 Cybernetics (Vol. 4, pp. 2395-2400). IEEE.

783 Yaseen ZM, Jaafar O, Deo RC, Kisi O, Adamowski J, Quilty J, El-Shafie A. 2016. Stream-flow
784 forecasting using extreme learning machines: a case study in a semi-arid region in Iraq. *Journal of*
785 *Hydrology* 542, 603-614

786

787 **Supplementary information material**

788 Table A. Optimum values of each model's parameter

Models parameters	Developed algorithms						
	ISOR	SMOR	LWL	ICO	LMS	Dagging	RS
Debug	No	-	NO	NO	No	No	NO
C	-	1	-	-	-	-	-
Filter type	-	Normalize training data	-	-	-	-	-
Kernel	-	Poly-kernel	-	-	-	-	-
Reg-optimized	-	Reg-SMO Improved	-	-	-	-	-
KNN	-	-	-1	-	-	-	-
Nearest Neighbor search algorithm	-	-	Linear NN Search	-	-	-	-
Weighting Kernel	-	-	0	-	-	-	-
Random seed	-	-	-	-	0	-	-
Sample size	-	-	-	-	4	-	-
Classifier	-	-	-	-	-	ISOR, SMOR, LWL, ICO, LMS	ISOR, SMOR, LWL, ICO, LMS
Number of folds	-	-	-	10	-	10	-
Verbose	-	-	-	-	-	No	-
SubSpace size	-	-	-	-	-	-	0.5
Batch size	-	-	-	100	-	-	-
Class value index	-	-	-	-1	-	-	-
Do not check capability	-	-	-	No	-	-	-
Evaluation metric	-	-	-	<i>RMSE</i>	-	-	-
Iterative classifier	-	-	-	Additive regression	-	-	-
Look ahead iterations	-	-	-	50	-	-	-

789

790

791 Table B. definition of each models parameter

Parameters	definition
Debug	Is set to yes, classifier may output addition information to the console
C	The complexity parameter C
Filter type	Determines how/if the data will be transformed
KNN	How many neighbors are used to determine the width of the weighting function
Weighting Kernel	Determines weighting function
Random seed	Set the seed for selecting random subsamples of the training data
Sample size	Set the size of random samples used to generate the least squared regression functions
Number of folds	Number of fold for cross-validation
Verbose	Whether to output some additional information during building
SubSpace size	Set of each subspace: if less than 1 as a percentage of the number of attributes, otherwise the absolute number of attributes
Batch size	The preferred number of instances to process if batch prediction is being performed
Class value index	The class value index to use with information retrieval type metrics
Do not check capability	If set to yes, classifier capabilities are not checked before classifier is built
Evaluation metric	Evaluation metric to use
Iterative classifier	The Iterative classifier to be optimized
Look ahead iterations	The number of iteration to look ahead for to find a better optimum

792